RESEARCH ARTICLE

Composition of freshwater in the spring of 2014 on the southern Labrador shelf and slope

M. Benetti[1,2] [ID]**, G. Reverdin[1], C. Lique[3]** [ID]**, I. Yashayaev[4]** [ID]**, N. P. Holliday[5]** [ID]**, E. Tynan[5], S. Torres-Valdes[5], P. Lherminier[3]** [ID]**, P. Tréguer[6], and G. Sarthou[6]**

[1]Sorbonne Universités (UPMC, Univ Paris 06)-CNRS-IRD-MNHN, LOCEAN Laboratory, Paris, France, [2]Institute of Earth Sciences, University of Iceland, Reykjavik, Iceland, [3]Ifremer, Univ. Brest, CNRS, IRD, Laboratoire d'Océanographie Physique et Spatiale (LOPS), IUEM, F-29280, Plouzane, France, [4]Department of Fisheries and Oceans, Ocean Sciences Division, Bedford Institute of Oceanography, Dartmouth, Nova Scotia, Canada, [5]National Oceanography Centre, Southampton, UK, [6]Laboratoire des Sciences de l'Environnement Marin (UMR 6539 CNRS/UBO/IRD/Ifremer), Plouzané, France

Abstract The Labrador Current is an important conduit of freshwater from the Arctic to the interior North Atlantic subpolar gyre. Here we investigate the spatial variability of the freshwater sources over the southern Labrador shelf and slope during May–June 2014. Using measurements of seawater properties such as temperature, salinity, nutrients, and oxygen isotopic composition, we estimate the respective contributions of saline water of Atlantic and Pacific origins, of brines released during sea ice formation, and of freshwater from sea ice melt and meteoric water origins. On the southern Labrador shelf, we find a large brine signal and Pacific water influence indicating a large contribution of water from the Canadian Arctic. The brine signal implies that more than 4 m of sea ice formed upstream, either in the Arctic or in Baffin Bay and the northern Labrador Sea. Over the midshelf and slope at 52°N, we find a stronger influence of slope water from the West Greenland Current with a smaller contribution of Pacific water and no brine signal. Thus, there is advection of water from the slope region to the midshelf between 55°N and 52°N. Very freshwater with high meteoric content is found close to the coast in June 2014. Observations from 1995 and 2008 suggest a higher fraction of brine and Pacific water on the shelf compared to that observed in 2014.

1. Introduction

The Labrador shelf and upper slope are major pathways of freshwater from the Arctic to the North Atlantic subpolar gyre. Its freshwater penetrates the gyre at the surface close to its southern rim south of 50°N [*Fratantoni and McCartney*, 2010; *McGeehan and Maslowski*, 2011]. The pathway to the Labrador Sea interior is less direct, with the exception of some sea ice flux from the northwestern shelves of the Labrador Sea [*McGeehan and Maslowski*, 2011]. In contrast, the west Greenland shelf and slope appear to be major sources of freshwater to the Labrador Sea interior [*Lilly et al.*, 1999; *Straneo*, 2006]. The freshwater in the Labrador Sea interior can get mixed down to the intermediate layers via intermittent deep convection [*Lazier et al.*, 2002; *Yashayaev and Loder*, 2009; *Yashayaev et al.*, 2007]. Varying freshwater inputs through these two shelf and slope regions influence convection in the Labrador Sea [*Lazier*, 1973], and possibly long-term variability of the world ocean circulation [*Rahmstorf et al.*, 2015]. Various multiyear freshening episodes have occurred since the late 1960s [*Reverdin*, 2003; *Yashayaev*, 2007; *Yashayaev et al.*, 2015], with the latest starting in the early 2010s and continuing into the present. Episodes such as the Great Salinity Anomaly [*Dickson et al.*, 1988] have been attributed to changes in outflow from the Arctic and are probably caused by a particularly large freshwater (and sea ice) flow through Fram Strait [*Belkin et al.*, 1998]. Other events might also be related to changes in the outflow from the Arctic through the Canadian Arctic and Baffin Bay [*Yashayaev*, 2007], whereas recent large increases in meltwater originating from the Greenland ice sheets or the Canadian glaciers since 2000 [*Shepherd et al.*, 2012] could have contributed to increased freshwater input through the shelf and slope currents.

In this paper, we examine the characteristics of water on the southern Labrador shelf and slope in order to establish the sources and pathways of freshwater. The ocean circulation in this region is characterized by a particularly fresh inshore current and a larger surface-intensified current above the shelf Break that bring water from higher latitudes. The inshore current lies close to the coast and downstream is partially
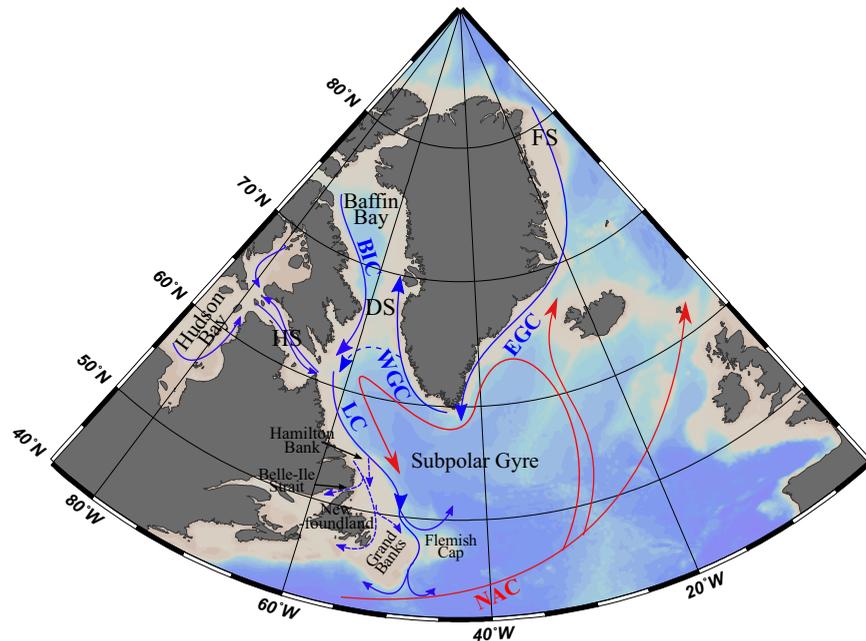
Figure 1. Schematic surface circulation in the Northern North Atlantic. Blue arrows are for cold and fresh currents; red arrows for warm and saline currents. NAC: North Atlantic Current, EGC: East Greenland Current, WGC: West Greenland Current, BIC: Baffin Island Current, LC: Labrador Current, FS: Fram Strait, DS: Davis Strait, and HS: Hudson Strait.

transported through Belle-Ile Strait to the Gulf of Saint-Laurence [*Petrie et al.*, 1988; *Mertz et al.*, 1993], and partially continues southward along Newfoundland (see Figure 1). The outer current follows the shelf break from the outlet of Hudson Strait (60°N) to Hamilton Bank (55°N) and then becomes wider further south, with some moving onto the shelf before rejoining the slope current just north of Flemish Pass [*Wu et al.*, 2012]. There is sparse published information on the sources of the Labrador shelf and slope waters; however, *Straneo and Saucier* [2008] suggest that freshwater in the inshore current originates from Hudson Bay, Baffin Bay, and the Canadian Arctic, whereas water further offshore is mainly recirculated water from west Greenland. Freshwater can be added through excess melt of advected sea ice or removed through excess formation of sea ice. Finally, the shelf can receive more freshwater from rivers and continental ice and snow-melt from Greenland or the Canadian Arctic.

Identifying contributions from different freshwater sources to the Labrador Current and Labrador shelf waters is a difficult undertaking [*Myers et al.*, 1990]. Measuring the water isotopic composition in seawater provides one of a few possible solutions to this problem, as different sources have specific isotopic compositions that can be traced/followed downstream. Such an approach was adopted for example in the study of *Khatiwala et al.* [1999] suggesting from an analysis of 1995 shelf data that up to 3 m of sea ice formation and export have taken place upstream of Newfoundland. 1994–1995 were years of large sea ice formation in the Labrador Sea (before the recent excess melt from Greenland and Canadian Arctic land ice). It also followed years of particularly large deep convection in the Labrador Sea and adjoining areas [*Yashayaev*, 2007], and relatively cold and fresh waters throughout the region. Another cruise provides isotopic data over the Labrador shelf in the summer 2008 [*Bacon et al.*, 2010], following formation of a relatively deep modification of the Labrador sea water [*Yashayaev and Loder*, 2009] and above-average winter sea ice cover [*Våge et al.*, 2011]. Here the main focus will be on data sets from three recent cruises (HUD2014007, JR302, GEOVIDE) in late spring 2014 over the south Labrador shelf and slope. 2014 is the first year with major sea ice cover since the mid-1990s and it experienced renewed deep convection in the Labrador Sea [*Kieke and Yashayaev*, 2015]. However, it follows a series of rather warm years and large excess sea ice melt in the Arctic and land ice melt over Greenland. We use temperature, salinity, nutrient, and δ^{18}O data from CTD (cond-temp-depth) profiles and water samples, to quantify the freshwater contribution of sea ice melt (SIM) and meteoric water (MW), Atlantic water (AW), and Pacific water (PW). MW includes precipitation (rain and snow) over the ocean, river runoff, and continental ice cap melt. We adopt the approach of earlier studies

based on mass balance calculations, such as those for Davis Strait sections [*Azetsu-Scott et al.*, 2012], Fram Strait sections [*Dodd et al.*, 2012; *Rabe et al.*, 2013], or the East Greenland Current sections [*Sutherland et al.*, 2009; *Cox et al.*, 2010; *Steur et al.*, 2015]. The emphasis here is on the spatial variability of the freshwater sources over the shelf and slope between 52°N and 55°N, as well as near-surface changes over the short period separating the three cruises (less than 45 days). This will be compared with two earlier near-repeat sections of AR7W (see HUD2014007), HUD95011 in June 1995, and D332 in August 2008 to investigate temporal variability. Outputs from a numerical simulation will be used to place the hydrographic and tracer observations from the three cruises in the context of varying freshwater transport from the Arctic. A companion paper [*Benetti et al.*, 2016] has investigated seasonal surface data sets collected further south on the Newfoundland shelf and slope and suggested a change due to sea ice formation (brine signal) between 1994–1995 and 2012–2016. Here the investigation of vertical structure and on possible spring changes is used to shed further light on the long-time changes since the mid-1990s and variations of freshwater composition with depth.

2. Data

2.1. Cruises and Sampling

In this study, we use data derived from samples collected during three cruises across the southern Labrador shelf and slope in 2014 (Figure 2). In addition, we use data from samples collected on the west Greenland shelf and slope from the cruise in May 2014, as a reference of water composition of this upstream freshwater to the Labrador current. The first cruise HUD2014007 took place in early May 2014 on R/V Hudson [*Yashayaev et al.*, 2015], crossing the shelf slope offshore of Hamilton Bank (AR7W section). Due to the presence of sea ice near the coast on 13 May, the cruise did not sample the 50 km closest to the coast. Sampling also included the southwestern Greenland shelf and slopes (see Figure 2). The second cruise, JR302 on RRS James Clark Ross [*King et al.*, 2015], crossed the shelf area near 52°N on 8–10 June starting close to Belle-Isle Strait before a transect through the Labrador Sea. The last cruise GEOVIDE (DOI10.17600/14000200) followed a similar route to JR302 (starting from west Greenland), reaching the Labrador shelf on 25–26 June. Due to limited time, samples were collected from only four stations on the shelf, the last station being south of the JR302 cruise. Further cruise information is provided in Table 1. Nutrient (NO_2, NO_3, PO_4, and silicates) data were collected on most stations with at least 10 measurements over the top 150 m, an appropriate resolution for our purpose. Qualified ammonium data were obtained on the JR302 and GEOVIDE cruises. Water isotope sampling is often more limited in the vertical on the shelf and slope stations, but in all cases with at
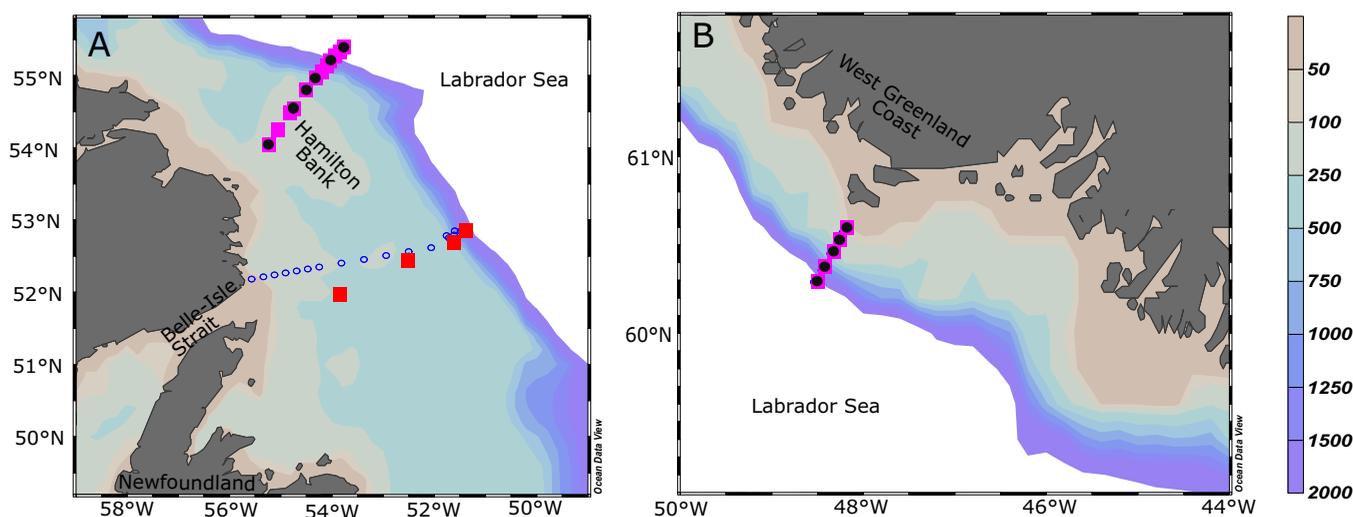
Figure 2. (a) Map of southern Labrador shelf and slope 2014 CTD and water sampling stations from the 2014 occupation of the HUD2014007 (magenta square), JR302 (blue dot), and GEOVIDE (red square) cruise. Vertical profiles of temperature and salinity are available for each CTD stations. For HUD2014007 cruise, the black dots indicate CTD stations in which $\delta^{18}O$ measurements have been done. During JR302 cruise, $\delta^{18}O$ measurements were done at every other station, starting by the most inshore station. During GEOVIDE, $\delta^{18}O$ have been measured for each of the four stations. For the three cruises, nutrient concentrations were measured on most stations. (b) 2014 HUD2014007 stations on the West Greenland shelf and slope. The bathymetry contours are drawn until 2000 m.

Table 1. Main Characteristics and Measurements of the Five Cruises Sampling the Labrador Shelf and Slope in 1995, 2008, and 2014

Cruise ID	Ship	Dates	Section	Samples	Data Corrections
Hudson 95011	CSS Hudson	11 Jun 1995	AR7W	NO_2, NO_3, PO_4, $\delta^{18}O$	$\delta^{18}O$ adjusted by $-0.15‰$
D332	RRS Discovery	22–25 Aug 2008	AR7W	NO_2, NO_3, PO_4, $\delta^{18}O$	$\delta^{18}O$ adjusted by $-0.15‰$
HUD2014007	R/V Hudson	13 May 2014	AR7W	NO_2, NO_3, PO_4, $\delta^{18}O$	No correction
JR302	RRS James Clark Ross	8–10 Jun 2014	52°N (full shelf)	NO_2, NO_3, PO_4, NH_4, $\delta^{18}O$	$\delta^{18}O$ corrected from evaporation (Appendix A)
GEOVIDE	Pourquoi pas?	25–26 Jun 2014	52°N (middle and outer shelf)	NO_2, NO_3, PO_4, NH_4, $\delta^{18}O$	No correction

least one sample close to the surface, and one in the cold subsurface layer between 50 and 100 m (typically, 6, 4, 3 samples were collected in the top 100 m for GEOVIDE, JR302 and HUD2014007, respectively). We also use data from two earlier AR7W sections in June 1995 (HUD95011) and in August 2008 (D332), during which nutrients and oxygen isotopes have been measured.

2.2. Measurement Methods

Vertical temperature (T) and salinity (S) profiles were measured with a SBE 911 plus CTD mounted on a rosette sampler on all cruises. The instruments were calibrated before and after each cruise. Additionally, measurements were calibrated with salinity samples analyzed on salinometers referenced to standard sea water. The accuracy in S is 0.002, the international GO-SHIP standard (www.go-ship.org) (we express S in the practical salinity scale of 1978, pss-78, with no unit). Water samples were collected using a 24-bottle rosette equipped with Niskin bottles. Nitrate, nitrite, and phosphate have been measured for the three cruises. Samples were collected in polypropylene 250 mL bottles and were analyzed using colorimetric methods against international standards (RMNS KANSO Techos LTD Japan). In both JR302 and HUD2014007 cruises the nutrient samples were analyzed on board. During GEOVIDE, most of the nutrient samples were analyzed on board but due to technical problems some samples were frozen and phosphate and nitrite were also analyzed afterward (accuracy: ±0.1 μmol N NO_3 kg^{-1}; ±0.01 μmol N NO_2 kg^{-1}). We used ammonium measurements from JR302 and GEOVIDE cruises, but not from HUD2014007 collected earlier in the season when measured levels were usually very low. During GEOVIDE, ammonium was analyzed from samples frozen at $-18°C$ (accuracy: ±0.01 μmol N kg^{-1}).

During JR302, water samples for $\delta^{18}O$ measurement were collected in 5 mL screw top vials, sealed with parafilm and electrical tape. During the HUD2014007 and GEOVIDE cruises, water samples for oxygen isotopes were collected in 30 mL tinted glass bottles (GRAVIS). The samples have been analyzed with a PICARRO CRDS (cavity ring-down spectrometer; model L2130-I Isotopic H_2O) at LOCEAN-IPSL (Paris, France). Based on repeated analyses of an internal laboratory standard over several months, the reproducibility of the $\delta^{18}O$ measurements is $\pm0.05‰$. The analyses were performed by running six injections per sample. The first three injections are ignored to eliminate potential memory effects between samples. The remaining three injections are averaged and calibrated against two internal water references) ($-0.05‰$ and $-3.26‰$ VSMOW). All reference waters are stored in steel bottles with a slight overpressure of dry nitrogen to avoid evaporation and exchanges with ambient air humidity. These references have been calibrated using IAEA references (GISP and SMOW) and several internal standards from other laboratories have been used to confirm these calibrations. All seawater samples have been distilled to avoid salt accumulation in the vaporizer and its potential effect on the measurements [e.g., *Skrzypek and Ford*, 2014].

The $\delta^{18}O$ values of samples of the 1995 cruise were analyzed at the Lamont Doherty Earth Observatory (LDEO) on a GV Instruments Isoprime dual inlet IRMS coupled with Aquaprep sample preparation system, and in 2008 at National Oceanographic Center on a similar instrumentation. These analyses were performed by equilibrating the seawater sample with a reference CO_2 gas of known $\delta^{18}O$ value. We found differences in duplicate samples measured on a Picarro at LOCEAN and in other laboratories. Because of the methodological effect and possible changes in the Atlantic surface seawater composition, we adjusted the data based on the comparisons presented in *Benetti et al.* [2016]. Although the origin of this offset is still not fully understood, we apply an offset of $-0.15‰$ to the 1995 and 2008 $\delta^{18}O$ measurements done with IRMS-Aquaprep to compare them with the 2014 measurements done with the CRDS at the LOCEAN. As this adjustment is constant and affects all end-members, it does not affect the calculation of the water source fractions (see section 3.2).

The 2014 samples also provide a measurement of δD. Here we use the relation between deuterium excess (d-excess = **δD-8*δ**^{18}O [*Dansgaard*, 1964]) and salinity to assess whether samples evaporated during storage (see Appendix A). Two thirds of the samples from JR302 that were stored for almost a year in sealed tubes were found to have evaporated. This resulted in anomalously low d-excess (and too large δ^{18}O). We then used the relationship of d-excess versus salinity observed in the Labrador Current, to estimate this anomalous decrease of d-excess and relate it to the evaporative change in δ^{18}O. The method is fully described in Appendix A. When moderate changes in d-excess occurred, the method resulted in reasonable estimates of δ^{18}O. However, this adds an uncertainty of at least 0.1‰.

2.3. Drakkar ¼° Simulation

In order to provide a background on variability in ocean transports and exchange with the Arctic, we use monthly outputs from a realistic model simulation the ORCA025 Drakkar global ocean/sea-ice model run from 1958 to 2015 [*Lique et al.*, 2009]. The forcing data set is the Drakkar forcing set 5 (DFS5, which is an updated version of the fields described in *Brodeau et al.* [2010]). Outflows of continental water were modeled with a constant seasonal cycle, so this run simulates circulation, salinity, and freshwater changes forced by wind and buoyancy fluxes. Further details of the hindcast as well as validations with observations can be found in *Grégorio et al.* [2015] and *Barrier et al.* [2015]. In particular, the simulation has been validated in the Arctic and the exchanges with the North Atlantic subpolar gyre have been compared against various data records, which suggest that despite its relatively low resolution it resolves major components of the transport and its low-frequency variability [*Lique et al.*, 2009, 2010; *Lique and Steele*, 2013]. A comparison (not shown) with SSMI-derived sea ice cover maps provided at National Snow and Ice Data Center indicate that the sea ice simulation reproduces the timing of sea ice formation and melt in the Labrador Sea. The simulation circulation pattern over the Labrador and Newfoundland shelves presents the same structures as published current maps [*Wu et al.*, 2012].

3. Calculation of Pacific Water, Meteoric Water, and Sea Ice Melt Fractions

We adopt a widely used mass balance approach whereby water mass composition is separated into a sea ice melt (SIM) fraction (f_{SIM}), a meteoric water (MW) fraction (f_{MW}), and a seawater fraction. The seawater fraction is a combination of Pacific water (PW) and Atlantic water (AW). The ratio of the fractions of Pacific water (f_{PW}) and Atlantic water (f_{Aw}) is calculated based on the distinctive nitrogen to phosphorus (N-P) relationships for the two water masses [*Jones et al.*, 1998]. The principle is briefly summarized as follows. In the global ocean, the N:P ratio associated with biological production and regeneration of organic matter is usually around 16 [*Redfield*, 1958, 1963; *Falkowski and Davis*, 2004; *Arrigo*, 2005]. However, PW entering the Arctic Ocean across the Bering Strait is depleted in nitrate relative to phosphate compared to AW [*Jones et al.*, 2008; *Yamamoto-Kawai et al.*, 2008]. This depletion is due to denitrification processes occurring over the sediments on the Bering and Chuckchi shelves [*Cooper et al.*, 1997; *Jones et al.*, 1998]. In practice, f_{pw} is estimated as follows [e.g., *Sutherland et al.*, 2009]:

$$f_{pw} = \frac{N^m - N^{AW}}{N^{PW} - N^{AW}}, \tag{1}$$

where N^m is the measured dissolved inorganic nitrogen, N^{AW} and N^{PW} are the values for pure Atlantic and Pacific water estimated from *Jones et al.* [1998], respectively. N^{AW} and N^{PW} values are calculated by substituting the PO_4^m value in the equation of the pure AW and PW N-P lines from *Jones et al.* [1998] (the slopes are close to what is expected from Redfield N-P stoichiometry). N is the sum of nitrate, nitrite, and ammonium (ammonium is neglected for HUD2014007 as the cruise took place early in the bloom season). MW and SIM fractions have very low nutrient concentrations and are assumed to lie on the AW line. Authors using similar methods considered an uncertainty of 10–14% on the estimation of the AW and PW fractions [*Jones et al.*, 1998; *Sutherland et al.*, 2009; *Dodd et al.*, 2012; *Bauch et al.*, 2011; *Taylor et al.*, 2003].

Knowing f_{PW}, the fractions f_{SIM} and f_{MW} can be determined following the method of *Östlund and Hut* [1984]. Because δ^{18}O of sea-ice melt is high compared to δ^{18}O of MW and both sources have very low salinity, the δ^{18}O-S relationship is particularly useful to discriminate the influence of SIM and of MW on LC surface salinity. The equations to estimate the water mass balance are presented below

Table 2. Salinity and δ^{18}O Characteristics of the End-Members Used in the Mass Balance Calculations[a]

Water Mass	S (Mean Value)	δ^{18}O (Mean Value)	References
Atlantic water	35.0	0.18	This study
Pacific water	32.5	−1.00	*Cooper et al.* [1997] and *Woodgate and Aagaard* [2005]
Meteoric water	0.0	−18.40	*Cooper et al.* [2008]
Sea ice melt	4.0	0.50	*Melling and Moore* [1995] and *Östlund and Hut* [1984]

[a]The choice of the end-member properties and the sensitivity of the method to their uncertainties are fully described in *Benetti et al.* [2016, Appendix B].

$$f_{AW} + f_{PW} + f_{MW} + f_{SIM} = 1, \tag{2}$$

$$f_{AW} \cdot S_{AW} + f_{PW} \cdot S_{PW} + f_{MW} \cdot S_{MW} + f_{SIM} \cdot S_{SIM} = S_m, \tag{3}$$

$$f_{AW} \cdot \delta O^{18}_{AW} + f_{PW} \cdot \delta O^{18}_{PW} + f_{MW} \cdot \delta O^{18}_{MW} + f_{SIM} \cdot \delta O^{18}_{SIM} = \delta O^{18}_m, \tag{4}$$

where S_m and δO^{18}_m are the measured values. f_{AW}, f_{PW}, f_{MW}, and f_{SIM} are the relative fractions of AW, PW, MW, and SIM. A negative f_{SIM} indicates net formation of sea ice, while a positive fraction indicates net melting of sea ice.

The end-member values used in the mass balance calculations are reported in Table 2. How they were chosen within a range of likely values is fully discussed in *Benetti et al.* [2016] for conditions very close to what is found here and is summarized in the following. AW properties are typical for the Irminger Current flowing into the Labrador Sea from the Irminger Sea (estimated from the SURATLANT cruises [see *Benetti et al.*, 2016, Appendix B]). It is a little saltier and heavier (35 and 0.18 ± 0.05‰) than the water found below the surface layer in the interior of the Labrador Sea. The salinity and δ^{18}O of the PW have been set following the approach of *Dodd et al.* [2012]. We used a salinity of 32.5 (flow weighted mean salinity calculated by *Woodgate and Aagaard* [2005] and *Woodgate et al.* [2012]). The δ^{18}O value of −1‰ is determined from the relationship between S and δ^{18}O measured on the Bering Sea shelf [*Cooper et al.*, 1997, 2006]. Note that the S-δ^{18}O relationship from *Cooper et al.* [1997] does not take into account the Alaska Coastal Water, for which salinity is somewhat different than the mean salinity provided by *Woodgate and Aagaard* [2005] based upon year-round measurements across the whole Bering Strait. For sea ice, we used an average salinity of 4 [*Östlund and Hut*, 1984] and a value of δ^{18}O = +0.5‰ (we apply the isotopic fractionation between liquid and solid to the mean δ^{18}O value of the Arctic Ocean [*Östlund and Hut*, 1984; *Melling and Moore*, 1995]). Larger uncertainties exist in the δ^{18}O value of MW, in part because precipitation measurements during the full year over the Arctic Ocean are lacking. Moreover, in the region we consider, MW also contains continental ice cap melt and snowmelt with considerable spatial and interannual variations, so that an overall synthesis is not possible. Local input of MW along the Labrador coast can also contribute to a lesser extent. Here we set the $\delta^{18}O_{MW}$ to −18.4‰, but consider that variations between −18 and −21‰ are conceivable.

Sensitivity tests have been done in *Benetti et al.* [2016] to evaluate the impact of the uncertainties on the calculation of water mass fractions. There is little impact on the fraction calculations related to the SIM properties, and more sensitivity to the end-member $\delta^{18}O_{MW}$. The fraction f_{MW} is also sensitive to the PW properties and to the proportion AW:PW to roughly 1%, but the effect is weaker on f_{SIM}. Thus, the largest uncertainties of this method reside in the choice of PW properties, MW δ^{18}O value, and PW/AW ratio and could have an effect on the order of 1% on the MW and SIM fractions. Most commonly, other similar studies have suggested uncertainties of 1–2%, in agreement with the sensitivity tests presented in *Benetti et al.* [2016]. Notice that despite strong uncertainties on the MW δ^{18}O value, this would not affect relative variations of the MW and SIM fractions between the different sections as long as the MW δ^{18}O value does not change. This assumption probably holds for the three sections of May–June 2014 but will be discussed later for the comparisons between the sections in the different years 1995, 2008, and 2014.

4. Spatial Distribution of the Freshwater During 2014

4.1. Salinity and Temperature Sections

We present the HUD2014007 and JR302 sections of salinity (S) and temperature deviation from freezing point (calculated at S = 33 and at the surface) (Figure 3). A small deviation of temperature from freezing
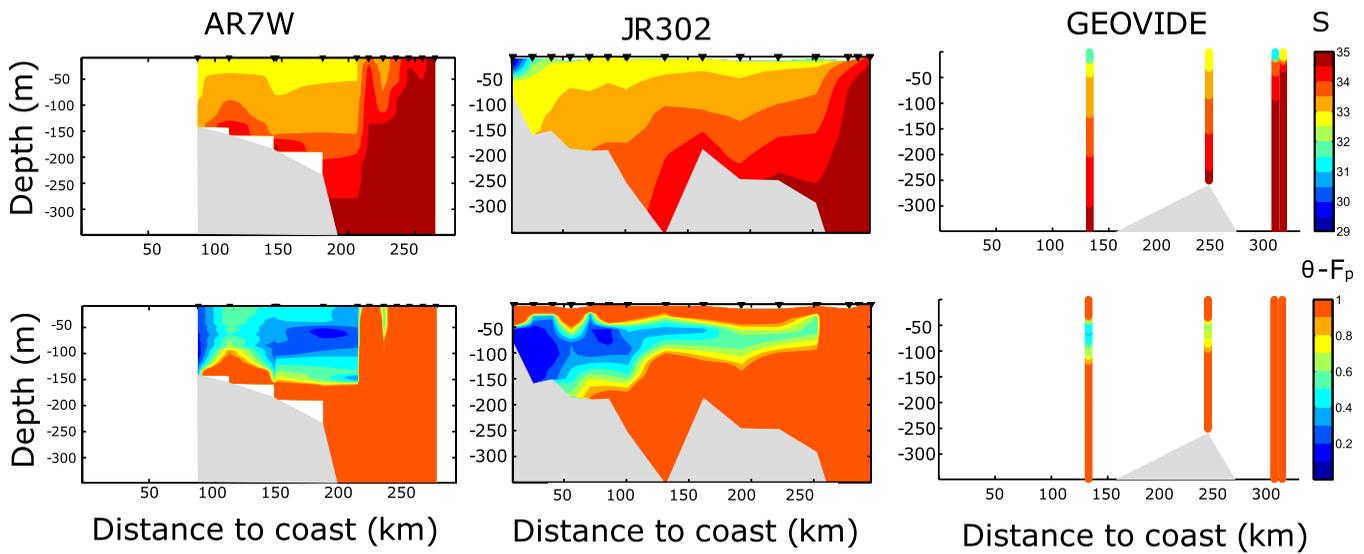
Figure 3. Section of salinity (top) and difference of potential temperature with the freezing point temperature calculated at S = 33 (bottom) (color scale for temperature differences less than 1°C). From left to right, HUD2014007, JR302, and GEOVIDE cruise. Only vertical profiles are presented for GEOVIDE, due to the limited number of CTD stations.

point temperature suggests the presence of brines released through sea ice formation during the previous winter. Low S on the order of 33 is found on the HUD2014007 section over the shelf and slope in a layer extending from 100 to 150 m, and shoaling across the slope. This water close to surface freezing temperature (see the 0.4°C difference contour) follows complete ice cover on this part of the Labrador shelf in April. There is just one station at 110 km from shore with slightly warmer and saltier water. Saltier and warmer water is found below this near-freezing water on the shelf. On JR302 section, 25 days later, the near S = 33, cold layer is found at subsurface over the shelf, but is capped by fresher (by up to −0.5) and warmer surface water. There is also a slight increase in subsurface S of this section on the outer part of the shelf. Very freshwater is found (less than 31 in the top 50 m) at the station closest (10 km) to the Labrador Coast, with this low-S water also observed in a diluted way to the next stations at 26 and 40 km from the coast. Part of the difference with HUD2014007 is related to JR302 being further south, with apparent inflow of saltier subsurface water over the outer part of the shelf between the two sections. Furthermore, HUD2014007 did not sample the innermost part of the shelf due to the presence of sea ice. For the GEOVIDE cruise, Figure 3 presents also the vertical profiles without horizontal interpolation, as the four stations are not sufficient to draw a section. Very large additional surface freshening is found in the top 25 m on three of the four stations, with the largest change found on the stations over the slope, one of those having the lowest SSS of 31.06, but with very strong haline stratification between 9 and 12 m depth ($\Delta S \approx 2$).

4.2. Pacific Water Fraction

Figure 4 shows total dissolved inorganic nitrogen ($N = NO_3 + NO_2 + NH_4$) versus phosphate. In this diagram, assuming the pure Atlantic and Pacific lines are parallel, the relative distance of any point from the two lines
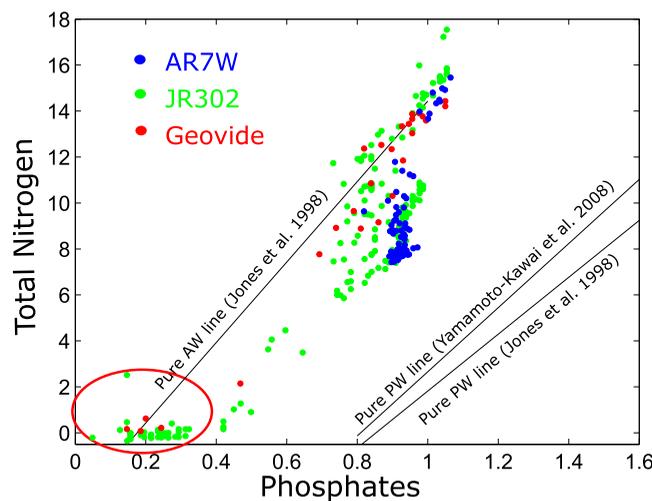
Figure 4. Total dissolved inorganic nitrogen (NO3 + NO2 + NH4) versus phosphate (μmol/kg). Colors are associated with cruises. Surface samples from JR302 and GEOVIDE (red circle) are strongly depleted in total dissolved nitrogen due to biological uptake. No such effect is observed during HUD2014007 cruise, earlier in the spring.
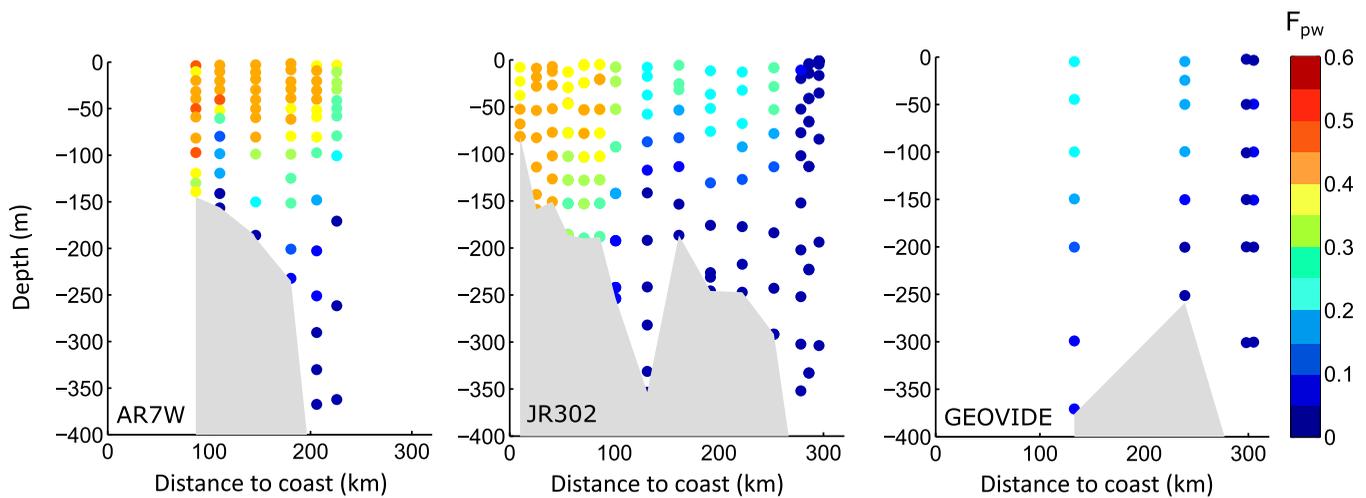
Figure 5. Spatial distribution of PW fractions derived from equation (1) for HUD2014007, JR302, and GEOVIDE cruises. The *x* axis is the distance to the coast in km. The *y* axis is the depth in m. Surface PW fractions for JR302 and GEOVIDE cruises have been extrapolated from deeper PW fractions (see Appendix B).

indicates the relative proportions between PW and AW. The ranges of nutrient values of the different data sets seem coherent in this region, with nutrient depletion in the stratified surface layer for the June cruises (JR302 and GEOVIDE), but not during the earlier mid-May HUD2014007 section. Based on the nutrient values, we derive from equation (1) the PW fractions for each section (Figure 5). The phosphate-depleted near-surface values in JR302 and GEOVIDE cruises lead to much lower surface f_{PW} than just below at the subsurface. This large change with respect to HUD2014007 in such a short time is unrealistic. Thus, we decided to replace the surface PW fractions on both June sections with the values estimated below. This correction is described in Appendix B. We also adjusted to 0 all negative PW fractions. Negatives values were located mostly over the continental slope where salinity was relatively high (negative PW fractions usually did not exceed -0.05 with four isolated low values near -0.2 for the JR302 cruise).

For HUD2014007, large PW fractions between 0.41 and 0.47 are observed across the shelf from the surface to 80–100 m, which corresponds roughly to the same layer with the lowest salinity and temperature. Below 100 m, there is also a rather cold layer but a little saltier (near 33.5) and much smaller f_{PW}. At 200 m, PW fractions are very low (<0.1), consistent with the saltier water found at that depth. On the shelf, the depth of penetration of PW increases toward the coast. There is a much larger across-shelf gradient in f_{PW} for JR302, with large fractions (between 0.41 and 0.45, same magnitude as in the HUD2014007 section) on the inner part of the shelf and lower fractions, but still significant, between 0.20 and 0.33 on the middle and outer part of the shelf in the upper 100 m. At the station closest to shore, fractions larger than 0.41 penetrate to the bottom, where very freshwater is still found. Over the middle and outer shelf, PW fractions are very low at 100–150 m (<0.1). The four stations of the GEOVIDE section have similar PW fractions compared to the nearby JR302 stations.

4.3. Meteoric Water and Sea Ice Fraction

The sea ice melt (SIM) and meteoric water (MW) fractions estimated from equations (2)–(4) are presented in Figure 6 along each section. The spatial distribution of f_{MW} follows a similar pattern on all three cruises, with an increase shoreward and to the surface where there is a freshening. Highest MW fractions are observed in the freshest surface waters of the interior shelf during JR302 at the stations closest to the coast with values of 0.11–0.12 and fractions remaining high at depth (two first stations, but no sample available below 70 m). In the minimum temperature layer, f_{MW} is typically on the order of 0.055 for the three cruises, with a decrease to 0.045 for the outer shelf stations, and further decrease to lower values in the slope region as salinity increases.

For f_{SIM}, we found -0.03 values on the shelf from 100 m to the surface in May 2014 (negative values indicate net brine rejection). The spatial distribution of the two June sections was different from the May section, with higher f_{SIM} values in total. In the subsurface layer, we also found -0.03 value but only in the inner shelf, then f_{SIM} increases to -0.02 in the outer subsurface shelf and to over than -0.01 for the slope of
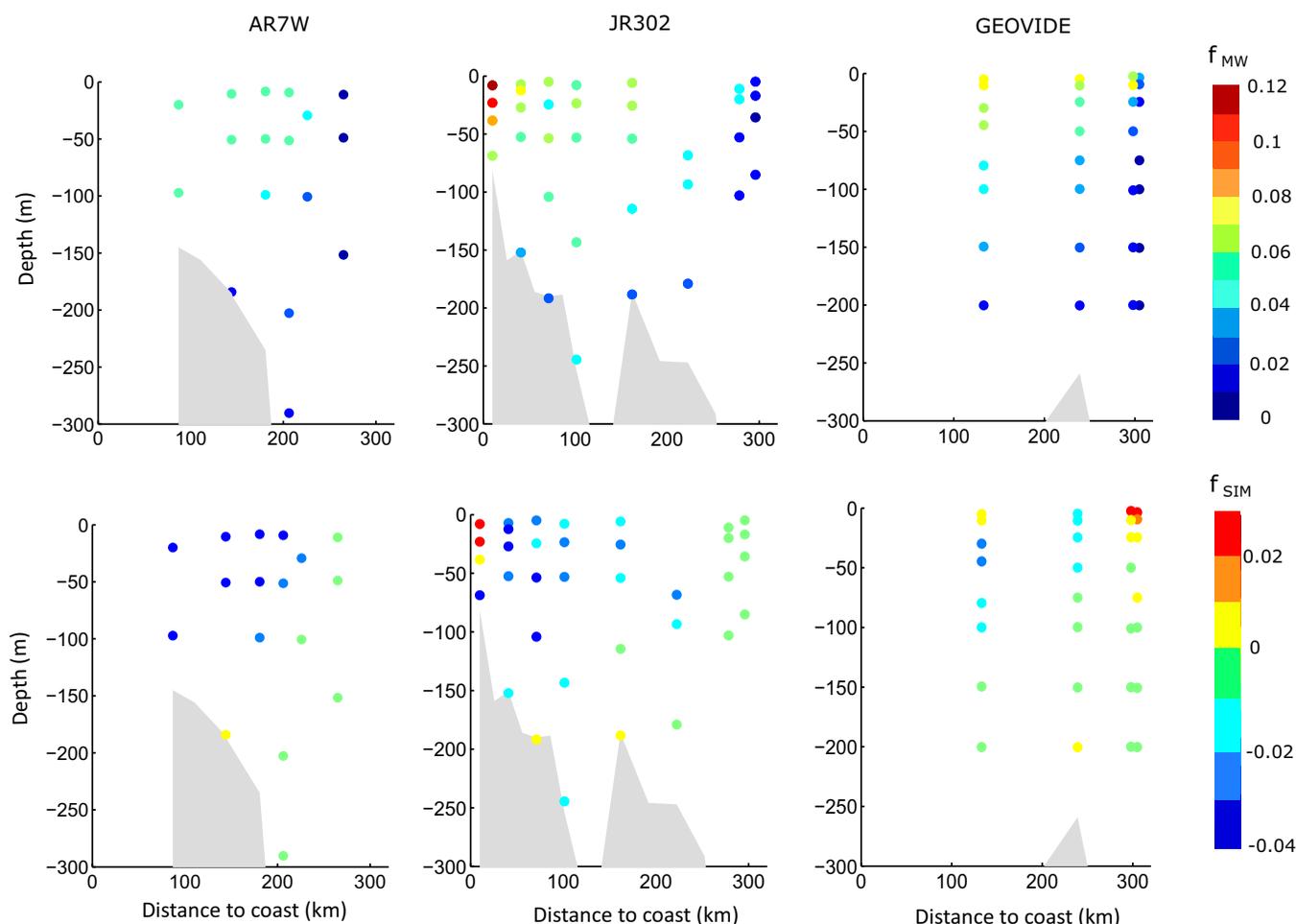
Figure 6. Fraction of meteoric water (f_{MW}) (top) and sea ice meltwater (f_{SIM}) (bottom) along the three 2014 sections: HUD2014007, JR302, and GEOVIDE.

JR302 and GEOVIDE. Near the surface, there is an increase in fSIM compared to the subsurface lower values, with the highest fractions found near the coast during JR302 and also for the two slope GEOVIDE stations.

4.4. Discussion

For the MW fractions, similar patterns are observed for the three cruises with an increase of f_{MW} toward the surface and the coast. This spatial distribution can be interpreted as an addition of freshwater, probably through advection from further north or from closer to the coast. In addition, JR302 is the only section that sampled the fresher near-coastal current with very large f_{MW} values (0.11–0.12) at the coastal station, but with similar PW fraction to shelf water further offshore. This is suggestive of a coastal current carrying freshwater from Baffin Bay, Hudson Bay, and local inputs along the Labrador Coast.

Then, the hydrological sections show a surface freshening and warming in June compared to May. We also notice higher SIM fractions at the surface in June compared to the same subsurface minimum observed in the three cruises. This is the signal of an increase in ice melt at the surface Labrador Current from mid-May to June. At the end of June 2014 (GEOVIDE section), the strongest positive fractions of SIM were observed over the continental slope and not on the shelf, and were trapped in a very shallow surface layer. This is where the strongest southward slope current was found (see further discussion and Figure 7), and is reminiscent of the sea ice melt patches observed near 49°N over the slope in July 2014 from ship-of-opportunity sampling [*Benetti et al.*, 2016]. The GEOVIDE stations being further upstream, this could be part of the same patch of freshwater. This indicates southward transport of sea ice meltwater in the LC, meaning that the LC provides a conduit for the exchange of freshwater of sea ice melt origin with the interior GSP (near Flemish Pass or further south) [*Fratantoni and McCartney*, 2010].
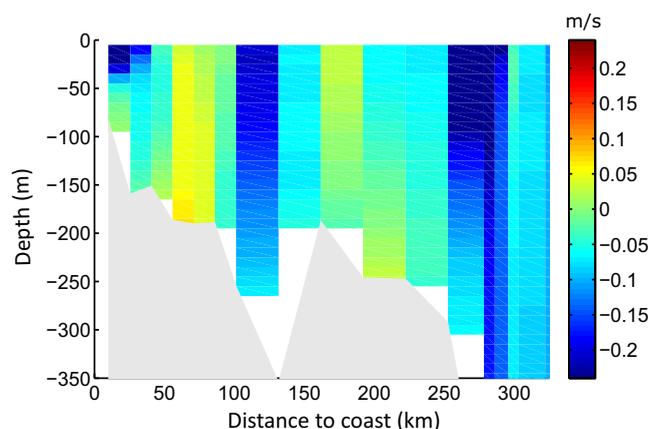
Figure 7. The current velocity (m/s) section from JR302 (based on geostrophy between stations adjusted to reference ADCP value). Near midshelf (100–130 km), the strong southward velocity station stands in the gradient separating the larger f_{PW} fraction water (and colder, slightly fresher water) found inshore from the water on the outer shelf.

Another interesting feature is the different spatial distribution of the PW fraction and brines at 55°N (HUD2014007) and 52°N (JR302 and GEOVIDE). Where do the PW and brines influence into the LC come from? The water on the west Greenland shelf of HUD2014007 (having transited across Fram Strait) was found to have f_{PW} only between 0.05 and 0.10, for a salinity that is between 33.2 and 33.5 (see Appendix B). In comparison, water having transited through the Canadian Arctic, as sampled in Davis Strait is much richer in PW [*Azetsu-Scott et al.*, 2012]. This water flowing from the Arctic through the Canadian Arctic and Baffin Bay (as seen in Davis Strait sections [*Azetsu-Scott et al.*, 2012]) has also a very negative f_{SIM} signature typical of the influence of brines, as there is much more near-surface water than sea ice exported from the Arctic in this region. It is different from Fram Strait, where f_{SIM} signature is near 0 [*Kwok and Rothrock*, 1999; *Sutherland et al.*, 2009]. We also found close to 0 values during HUD2014007 on the southwest Greenland shelf (not shown here, but the sampling is shown in Figure 1), where sea ice formation and melting seem to be approximately compensated. In short, the PW and brines distribution in the LC shows the proportion of water originating from the Canadian Arctic through Davis Strait compared to what originates from Fram Strait. High brine signal and PW fractions are indicative of a larger influence of waters having transited through Davis Strait, compared to low brine signal and PW fraction, indicating more influence of water carried by the WGC.

Thus, the large negative f_{SIM} values and large f_{PW} values that we observe in the LC in the three sections are probably originating to a large extent from the Canadian Arctic through Davis Strait. There is probably also a contribution of brines formed in the northern Labrador Sea/Baffin Bay, where sea ice is known to be partially exported to the interior of the Labrador Sea, whereas the near surface water enriched in brines remains over the shelf and along the slope as it drifts southward [*McGeehan and Maslowski*, 2011].

Moreover, the PW and brines distribution of the different sections suggest that the outer shelf near 52°N (and the subsurface shelf layer) presents a larger proportion of the freshwater from west Greenland poor in PW and brines, compared to the water closer to the coast at 52°N and over the shelf at 55°N, which would receive a larger fraction of water having transited through the Canadian Arctic and Davis Strait (higher PW and brines fractions). Notice that the relationships f_{SIM}-S and f_{PW}-S reveal both a slope break around S = 33.75, indicating the robustness of the f_{SIM} and f_{PW} calculations to trace waters from Baffin Bay and the Canadian Arctic against waters from Fram Strait (see Appendix C). This suggests a circulation that advects water close to the shelf break offshore of Hamilton Bank (55°N) onto the shelf further south (52°N), consistent with climatological surface currents [*Wu et al.*, 2012]. This shelf and slope circulation is also consistent with the Drakkar simulation and currents measured along the JR302 section, all of which have weak currents over parts of the shelf separated by strong localized surface intensified southward jets trapped by bathymetry (see the JR302 section in Figure 7). Near the coast there is a narrow surface jet of the very freshwater. There is a jet in the middle shelf (100–120 km) separating high PW, cold, freshwater from low PW, slightly warmer, and saltier water further on the outer shelf. This current might originate from the slope current near the HUD2014007 section, as suggested by climatological currents. Finally, we observe the strong slope current near the shelf break/over the upper slope on all sections.

5. Temporal Variability Between the Years 1995, 2008, and 2014

5.1. Integrated Contributions for 2014

We first derive an approximate relationship between f_{MW} and S, and between f_{SIM} and S, and then integrate them vertically to get an equivalent layer thickness of the different water components. These relationships

are presented in Appendix C. For f_{SIM}, we first estimate the contribution of ice formation by extrapolating the values in the minimum subsurface layer toward the surface, and then estimate ice melt by taking the difference of f_{SIM} with respect to the subsurface minimum that we relate to the salinity difference. These rough relationships are then integrated vertically using the CTD salinity profiles.

These estimates suggest that roughly 4 m of seawater has been extracted on the shelf to form sea ice along HUD2014007. This decreases to 2 m at the 225 km slope station and close to 0 m further offshore. We find 4.4 m according to the four inner stations of JR302. On the outer shelf (JR302 and GEOVIDE), the estimate is closer to 2 m, and decreases toward 0 m for the slope stations. Sea ice melt averages 0.5 m for the eight JR302 stations (but only 0.2 m if the coastal station is excluded) and 0.5 m for the four GEOVIDE stations. There is no detectable sea ice meltwater in HUD2014007. Thus, the sea ice melt signal is rather weak compared to the expected sea ice thickness in late winter, which for the first-year sea ice in the Labrador shelf as well as upstream in Baffin and Hudson Bays, is expected to have a thickness in the range of 0.7–1.3 m. This suggests that a significant part of the ice formed locally in the northern Labrador Sea is either not yet exported through the southern Labrador Sections, or is exported to the interior of the Labrador Sea further north, as suggested by modeling studies [*McGeehan and Maslowski*, 2011].

Integrating the meteoric water component vertically yields large uncertainties. We decided to integrate vertically down to S = 34.75, because, at higher salinity, the estimate is too strongly influenced by the uncertainties in the PW contribution and the choice of S = 35 for AW. On the shelf, this contribution is 9.4 m for the AR7W section, 10 m for the six JR302 stations, and 10.5 m for the two GEOVIDE stations. There is no particular difference between inner and outer shelf on JR302. For the five slope stations, this drops to 3.1 m. Stations further offshore in the southern Labrador Sea have MW contributions between 1 and 2 m. Thus, it includes both the large contribution of MW advected from the Arctic Ocean through Fram Strait and Davis Strait, as well as the freshwater input from Greenland, the Canadian Arctic, Hudson Bay, Labrador, and possible local excess precipitation over evaporation.

5.2. Comparison With Two Earlier Sections in June 1995 and August 2008

We apply the same methods to estimate the different water fractions for the two earlier AR7W sections in June 1995 and August 2008. Figures 8 and 9 present the spatial distribution of the PW, SIM, and MW fractions. Note that as for GEOVIDE and JR302, all surface nitrate values are depleted due to the biological uptake in the August 2008 section, and surface phosphate concentrations were unexpectedly low. Thus, we extrapolated PW fractions measured at subsurface to shallower depths (see Appendix B). These two sections suggest stronger inputs of PW in the LC compared to 2014 HUD2014007 section, with fractions between 0.50 and 0.60 over the continental shelf. In 1995 and 2008, PW spreads over the whole shelf without distinctive distribution between the inner and the outer shelf, although PW penetration is deeper close to the coast than it is in 2014 (HUD2014007). Some suspiciously large deep f_{SIM} values of August 2008 might
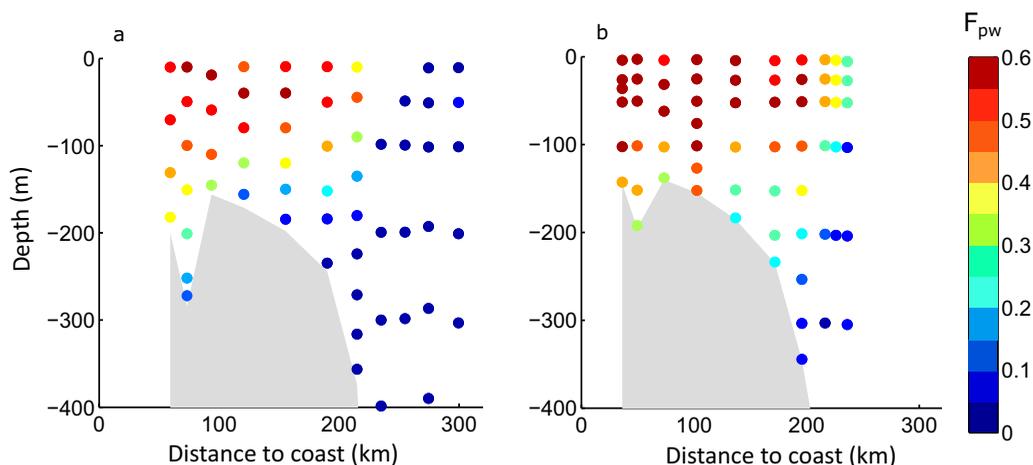
Figure 8. The spatial distribution of the PW fractions. (a) Section of June 1995, (b) section of August 2008, where surface PW fractions have been corrected according to the value at 50 m depth (see more details in Appendix B).
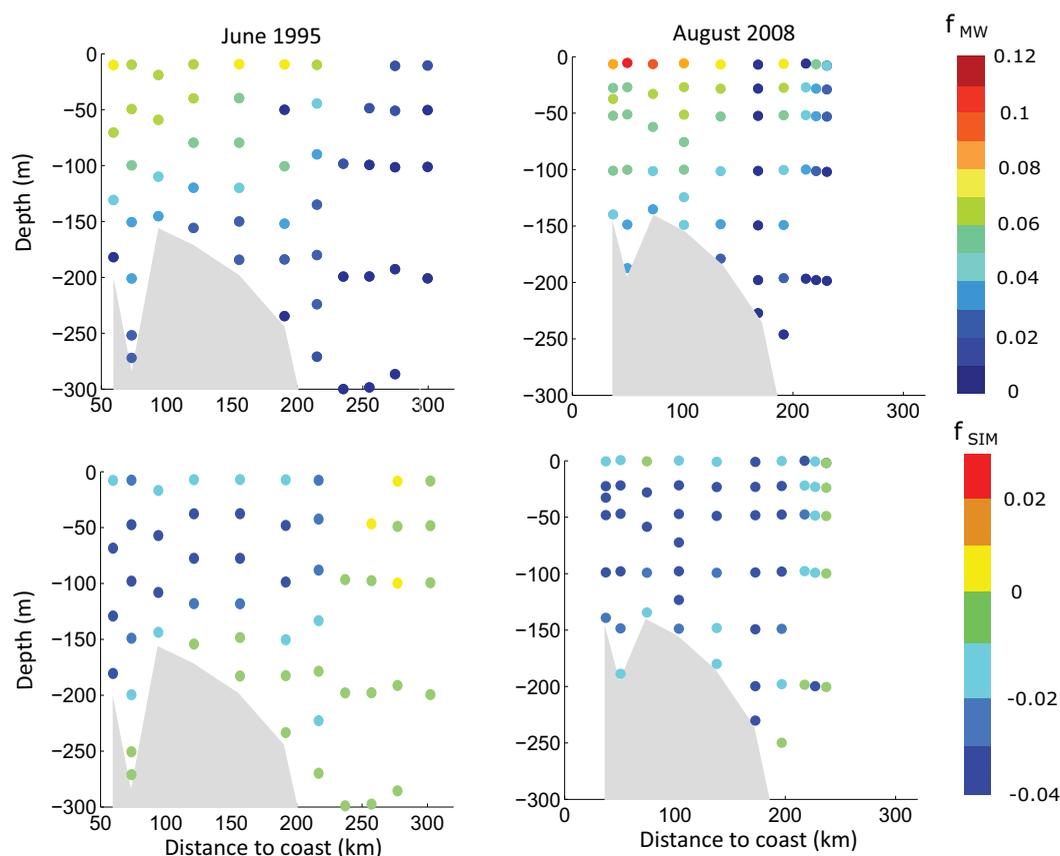
Figure 9. Fraction of meteoric water (f_{MW}) and sea ice meltwater (f_{SIM}) along the June 1995 (left) and August 2008 (right) sections. Top figures correspond to MW fractions. Bottom figures correspond to SIM fractions.

suggest lower accuracy for these samples. Large surface MW input, with fractions up to 0.11–0.12, is observed in August 2008 later in the melting season (Figure 9). During 1995 and 2008, f_{SIM} reaches −0.04 near 50 m depth over the whole shelf, increasing to −0.03 around 100 m. These values are more negative than in 2014, so that the estimated total ice formation amount is larger than in 2014, being 5.2 m in 1995 and 4.7 m in 2008. The sea ice melt is 0.6 m in 1995 and 0.5 m in 2008 over the shelf, and the total MW is 10 m in 1995 and 9 m in 2008: values fairly similar to the ones for 2014. In summary, the main differences between 1995/ 2008 and 2014 are in PW and in the total brine release (sea ice formation). *Benetti et al.* [2016] present surface data collected further south off Newfoundland during the 2012–2015 period, which also showed differences with earlier 1995 data. This was also interpreted as a reduction in brine signal in recent years. The interpretation of stronger brine release in the 1995 and 2008 sections could be altered if the δ^{18}O value of MW had changed between the sections. However, the larger PW input in 1995 and 2008 and the larger influence of brines are consistent with a stronger input from the Canadian Arctic in these earlier surveys.

5.3. Drakkar Freshwater Simulations

In the absence of published Davis Strait observations over the recent time period, we examine temporal variability in the Drakkar model simulation. The simulations suggest that interannual variability in freshwater transport at 55°N is fairly closely correlated with the Davis Strait freshwater transport, with a smaller contribution from the West Greenland Current freshwater (originating mostly from Fram Strait) (see Appendix D). The simulations suggest strong southward freshwater transport in 2014 near the AR7W section and upstream near Davis Strait. Transports are also large in 1995 near the AR7W section (at least in May/June), with lower values for the years in between. Figure 10a presents the average May–June salinity section at 55°N across which the southward freshwater transport is integrated. As in the observations, it presents freshest water at the surface near the shore, and a surface front just offshore of it. It also presents strong
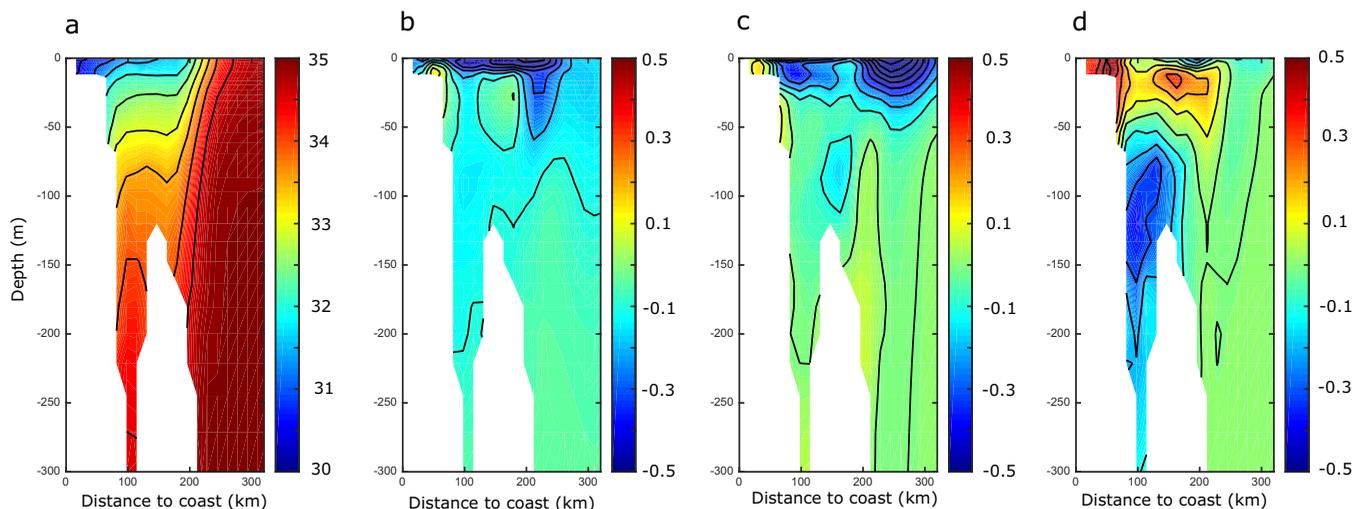
Figure 10. Average model May–June S section (0–300 m) across 55°N over the 1990–2015 period from Drakkar model. The S-anomalies are presented for 1995, 2008, and 2014, in Figures 10b–10d, respectively.

horizontal S gradients in the upper 200 m near the shelf break/upper slope. The S-anomaly sections are then presented for 1995, 2008, and 2014 (Figures 10b–10d). The S May/June anomalies at 55°N in the simulation tend to be negative in the 3 years (1995, 2008, and 2014), with largest negative anomalies at depth in 2014, compensated by positive anomalies near the surface. However, for these months, the simulation still presents sea ice in 2014, which could partially explain the S near-surface positive anomalies in May–June (brines) that are not found later in summer in the simulation.

Thus, altogether the simulations suggest that the 3 years are characterized by excess freshwater on the shelf originating mostly from excess freshwater transport across Davis Strait. They are not consistent with a reduction of this freshwater transport from the Canadian Arctic in 2014, as was suggested by the comparison of the sections f_{SIM} and f_{PW}.

6. Conclusions and Perspectives

The presence of a large brine signal in the LC over the shelf, even at the end of summer, and a fairly large proportion of Pacific water (PW fractions are between 0.20 and 0.50 in 2014, and up to 0.60 in 1995 and 2008), indicates the importance of the flow of water from the Canadian Arctic Archipelago over the southern Labrador shelf. The large brine signal in this upstream Arctic water might be increased by the export of sea ice from the northern shelves into the interior Labrador Sea. The lesser proportions seen over the outer shelf in JR302 and GEOVIDE sections at 52°N indicate a contribution of water from the WGC/EGC system which has no sea ice brine signal and little Pacific water. The penetration of this water onto the shelf south of AR7W where it is found near the shelf break is consistent with what is known of the shelf currents [*McGeehan and Maslowski*, 2011] and the currents measured along the JR302 sections. The very high MW fractions observed in the inner part of the Labrador shelf (0.11–0.12), with similar PW fraction to shelf water further offshore, reveal that the freshwater originates from local inputs, but also from the Baffin Island coastal current and Hudson Bay. The strongest positive fractions of SIM observed over the continental slope, as was also found near 49°N in July 2014 [*Benetti et al.*, 2016] indicate the transport of sea ice meltwater in the LC, which may then exchange this freshwater with the interior GSP near Flemish Pass [*Fratantoni and McCartney*, 2010].

The sections in 1995, 2008, and 2014 all followed winters with a positive NAO index, deep convection in the Labrador Sea and above-average sea ice extent. Thus, some of the local processes (sea ice formation, winter vertical mixing) present similarities in these different years. However, we found a large difference in the PW and sea ice formation contribution, with much lower influence in 2014. Indeed, we expect the LC properties to be rather sensitive to upstream changes in the properties and composition of flow through Davis Strait, which present significant interannual variability [*Curry et al.*, 2014; *Münchow*, 2016; *Michel et al.*, 2015]. In

these direct transport time series, 2008 does not appear as a very distinct year. However, the currently available time series across Davis Strait end up in 2010, and the Drakkar simulation also suggest strong freshwater transport across Davis Strait in 2014.

We also expect that the multidecadal decrease in sea ice thickness in the Arctic in recent years would result in a smaller brine signal (negative f_{SIM}) in the freshwater originating from the Arctic Ocean, in particular for the component transiting through the Canadian Arctic. However, this change should already be quite noticeable in 2008 [*Kwok and Rothrock*, 2009], which we do not observe (with the caveat that the 2008 section is much later in the year with a possible contribution of seasonal variability in transport sources). There have been recent increases in melt runoff from Greenland and the Canadian Arctic [*van der Broeke et al.*, 2016], but although this implies more meltwater contribution since the 1995 section, compared to the large inventory of MW on the shelf, the impact is probably still small.

We have estimated the uncertainties in our measurements and outlined those associated with the method. The uncertainties in PW properties and the extrapolation of subsurface f_{PW} to the surface induce uncertainties in the PW contribution, and indirectly, they also influence the MW contribution. Nevertheless, uncertainties in estimating SIM are smaller, even when separating an ice formation (brine release) signal based on subsurface data from a surface sea ice melt signal. The former in particular should be fairly relevant as a tracer of interannual variability. With the changing Greenland ice melt and other sources of meteoric water, we could expect the MW properties to vary significantly in time resulting in further uncertainties on how to compare sections collected under different climatic conditions. The uneven near-coastal sampling in different years for AR7W section could also result in irregular sampling of the freshest near-coastal water in the coastal current. Although its overall contribution to freshwater transport is probably small, it is nonetheless a matter of concern as it has a different MW contribution than water further from the coast on the shelf and slope, thus suggesting a different origin.

We expect that much more information could be retrieved from regular (annual) sampling both of upstream conditions in the west Greenland Current near Cape Farewell and across Davis Strait with AR7W sampling of the southern Labrador Sea and Shelf. Introducing water isotopic composition in model simulations such as Drakkar would also provide important diagnostic tools to interpret these data.

Appendix A: Extrapolation of Some Isotopic Values of the JR302 Section

Unfortunately, 15 samples from the JR302 section show signs of evaporation within their sealed tubes before they could be analyzed (they present unrealistically negative d-excess (d-excess $= \delta D - 8 \ast \delta^{18}O$ [*Dansgaard*, 1964]), lower than $-2\permil$ with largest value of $-6\permil$). For salinities ranging from 34.3 to 34.9, we estimated the biases $\Delta\delta^{18}O$ and Δd-excess due to the evaporation of the water sample from empirical relationships between d-excess and S and between $\delta^{18}O$ and S (see Figures A1a and A1b). The relationships are established using all the samples available over the Labrador shelf and slope between 0 and 400 (excluding JR302) and are not affected by sea ice processes for salinities ranging from 34.3 to 34.9. This establishes a linear relationship between Δd-excess and $\Delta\delta^{18}O$ (see Figure A1c). This linear relationship is then used to estimate the correction to apply to $\delta^{18}O$ in function of the Δd-excess of the evaporated sample. This method is possible because even for low salinity and the occurrence of sea ice melt, the relationship between d-excess and salinity holds rather well (see Figure A1b). Corrected $\delta^{18}O$-salinity relationship is shown in Figure A2 (see the spatial distribution of the corrected samples in Figure A3). The maximum applied correction is $-2.47\permil$. The largest error in the corrected estimate of $\Delta\delta^{18}O$ originates from the scatter in the relationship between d-excess and S.

Appendix B

Figures B1a and B1b present the spatial distribution of the PW fractions estimated from equation (1) using the raw nutrients values for JR302 and GEOVIDE. In June, the phosphate-depleted near-surface values in JR302 and GEOVIDE lead to unrealistic lower f_{PW} than just below in subsurface. No such feature is observed earlier in May during the HUD2014007 cruise. This strongly suggests that the Redfield ratios do not hold during biological processes in the nutrient-depleted surface layer, contrary to what is more usually observed in the Arctic Ocean [*Tremblay et al.*, 2015]. Thus, we chose to replace the surface estimates on both sections as follows: (1) JR302: we use f_{PW} estimated at 40 or 80 m (depending of the sampling) for all shallower
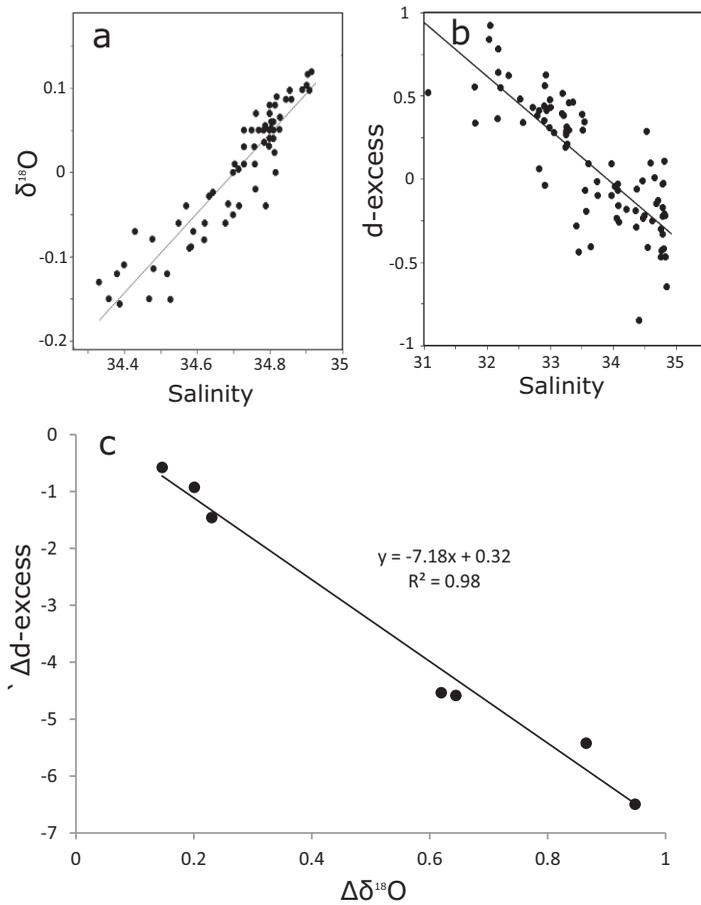
Figure A1. (a) δ^{18}O/S relationship in the Labrador shelf and slope between 0 and 400 m for salinity ranging from 34.3 to 34.9 (all data except JR302). The linear regression is δ^{18}O = 0.46*S-16.00. (b) d-excess/salinity relationship in the Labrador shelf and slope between 0 and 400 m and over the surface Labrador Sea for salinity ranging from 31 to 34.9 (all the data except JR302). The linear regression is d-excess = 0.34*S + 11.38. (c) $\Delta\delta^{18}$O/Δd-excess relationship (from samples with salinity ranging from 34.3 to 34.9). The linear regression is indicated in black (r^2 = 0.98).
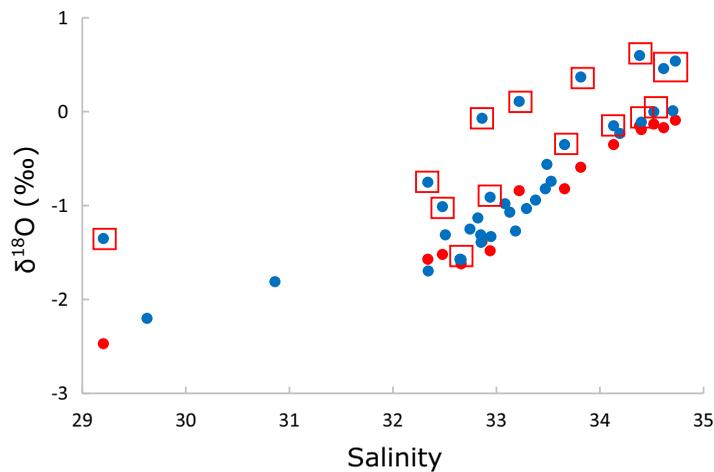
Figure A2. Fifteen evaporated samples (red box) were corrected using the relationship found in Figure A1c. The raw measurements are indicated in blue and the corrected samples in red.
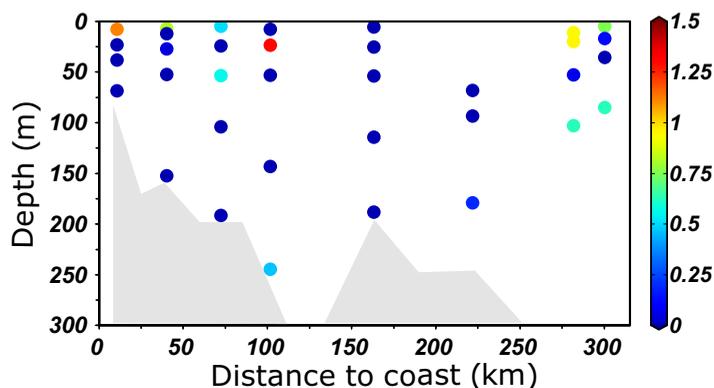
Figure A3. Spatial distribution of the evaporated samples. The amplitude of the correction is indicated with the colors (dark blue is used when no correction is applied).

samples. (2) GEOVIDE: we use the PW fraction estimated at 100 m to all shallower samples for the four stations. The new near-surface estimations of PW fractions have been adjusted by a factor of dilution proportional to the sample salinity. The final sections are presented in Figure 5. The low surface PW values could result from the dilution by higher input of SIM at the surface (assumed to have same nutrients properties as the AW). Nevertheless, the distribution of SIM fractions (not affected much by the PW/AW proportions) shows that this cannot explain alone the low PW fractions measured at the surface.

Figure B1c presents the spatial distribution of the PW fraction in the West Greenland Current in May 2014 from the HUD2014007 cruise. Most PW fractions in the WGC are between 5 and 10%. Figure B1d shows that surface depleted nutrients measured during August 2008 values led to unrealistic low PW fractions at the surface, as for GEOVIDE and JR302. To correct for that, we extrapolate PW fractions measured at 50 m to shallower samples (see Figure 8 with the corrected fractions).
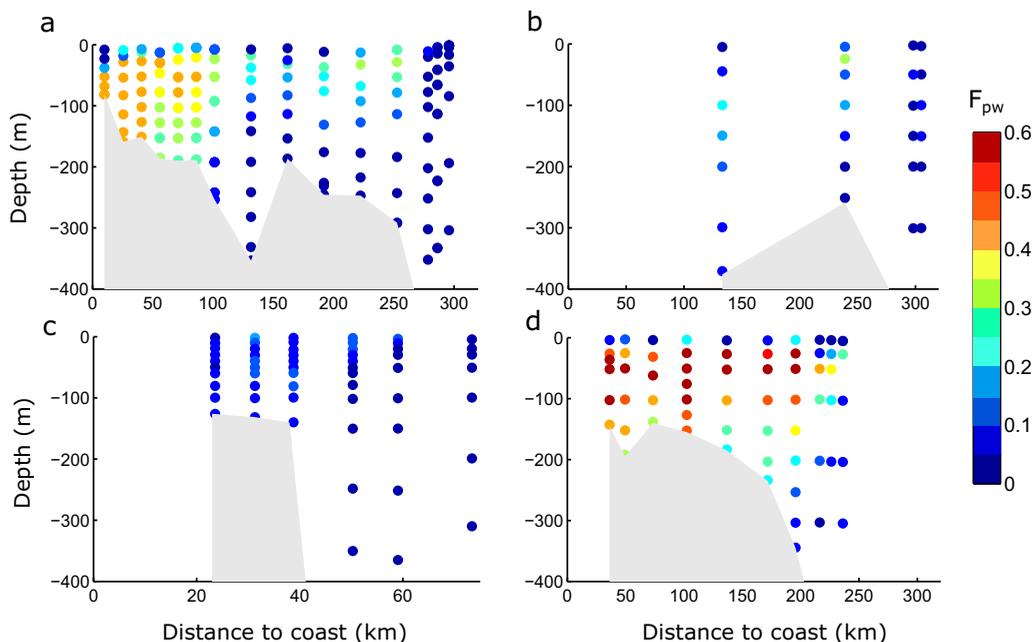
Figure B1. Spatial distribution of the PW fraction of (a) JR302 and (b) GEOVIDE from equation (1) using the nutrient measurement, without any extrapolation. Unexpectedly low PW fractions are observed in June at the surface. (c) Spatial distribution of the PW fraction from equation (1) using the nutrient measurement in the WGC in May 2014 (HUD2014007). See map in Figure 2 for the stations location (four closest stations to the coast). (d) Spatial distribution of the uncorrected PW fractions during August 2008. The color bar is the same as in Figures 5 and 6.
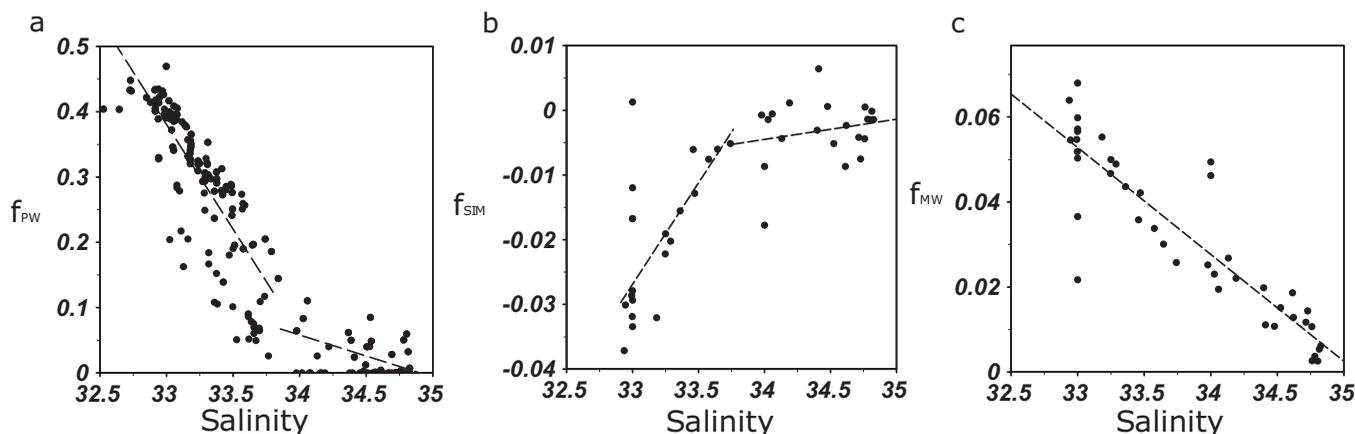
Figure C1. Relationship between salinity and the fractions of (a) Pacific water (f_{PW}), (b) sea ice melt (f_{SIM}), and (c) meteoric water (f_{MW}). The five linear regressions (black dashed line) are reported in Table C1. The sample at S = 33 and f_{SIM} = 0 has been removed to calculate the linear regression in the middle figure.

Table C1. Characteristics of the Five Linear Regressions Shown in the Figure C1

	Slope	Y Intercept	R
f_{PW} (S > 33.75)	−0.07	2.21	−0.53
f_{PW} (S < 33.75)	−0.32	10.88	−0.84
f_{SIM} (S > 33.75)	0.00	−0.11	0.20
f_{SIM} (S < 33.75)	0.03	−1.06	0.79
f_{MW}	−0.03	0.88	−0.90

Appendix C: Scatterplots

Figure C1 shows the evolution of f_{PW}, f_{SIM}, and f_{MW} as a function of S for the cruises in 2014 between 50 and 350 m (HUD2014007, JR302, and GEOVIDE). The relationships between S and f_{PW} or f_{SIM} reveal clearly a mixing with three poles: what comes from the Arctic and Baffin Bay, what comes from West Greenland shelf and upper slope, and AW properties. The linear regressions are indicated in Table C1. For both variables, the slope break appears at the same salinity around S = 33.75, confirming that SIM and PW are both efficient tracers of the water coming from the Arctic Canadian Archipelago. Thus, the diagrams reveal the strong influence of the water coming from the Arctic Canadian Archipelago in the fresher part of the Labrador Current, while for salinities higher than 33.75, the relationships reveal a stronger influence of water coming from the EGC and WGC system.

However, the f_{MW} distribution only shows two poles. It is also aligned with the data on the west Greenland shelf (not shown). As expected, the input of MW increases with decreasing salinity. But the unique relationship reinforces the assumption made in our mass balance calculations, of a common isotopic composition for MW. Stated differently, the data cannot contribute to distinguish isotopic compositions of the MW having flown along Greenland and of the MW originating from the Canadian Arctic.

Similar conclusions apply for the earlier cruises in 1995 and 2008, although the slopes and breakpoints are somewhat different (not presented).

Appendix D: Drakkar Freshwater Transport

Figure D1a presents integrated freshwater transport across 55°N on the Labrador shelf and slope in May–June of each year. In this season, the contribution of liquid freshwater dominates, although there is also some contribution of solid freshwater transport (noted ice), in particular in 2014. The total freshwater transport is indicated by the black curve. This figure illustrates large spring southward freshwater transport until 1996 and since 2012, with weaker transport in between (2003 and 2008 present local minima).

Figure D1b presents the monthly-averaged freshwater transport at 55°N (including both liquid and solid components) and the interannual variability is also identified by the 12 month smoothed curve. This model transport presents however less year-to-year variability which overlays a large seasonal cycle. The annual average follows rather closely the freshwater transport curve across Davis Strait (r = 0.42). The correlation coefficient is −0.07 between freshwater transport at 55°N and at Fram Strait. The annual average and the
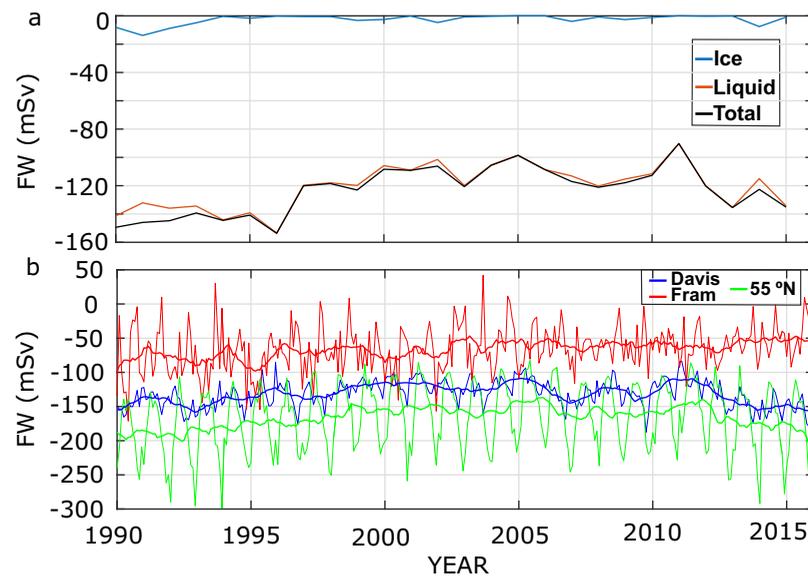
Figure D1. (a) Drakkar model May–June southward freshwater transport across a Labrador shelf and slope section at 55°N. Freshwater transport through the different sections is computed based on a reference salinity of 34.8 [*Aagaard and Carmack*, 1989], taking into account the part of the section where the flow is southward and salinity is lower than 34. Equivalent freshwater transport for sea ice is estimated using the constant sea ice salinity used in the simulation (6). (b) Monthly time series of freshwater transport across three sections: red at Fram Strait (between Greenland and Svalbard), blue across Davis Strait (between Baffin Island and Disko Bay), and green for the 55°N section. The thick curves correspond to a 12 month running average.

May–June averages also present similar multiyear evolution, although on a yearly basis they can be rather different (for example in 1996).

References

Aagaard, K., and E. C. Carmack (1989), The role of sea ice and other fresh water in the Arctic circulation, *J. Geophys. Res.*, *94*(C10), 14,485–14,498.

Arrigo, K. R. (2005), Marine microorganisms and global nutrient cycles, *Nature*, *437*(7057), 349–355.

Azetsu-Scott, K., B. Petrie, P. Yeats, and C. Lee (2012), Composition and fluxes of freshwater through Davis Strait using multiple chemical tracers, *J. Geophys. Res.*, *117*, C12011, doi:10.1029/2012JC008172.

Bacon, S. (2010), RSS Discovery Cruise 332, 21 Aug–25 Sep 2008. Arctic Gateway (WOCE AR7), *Natl. Oceanogr. Cent. Southampton Cruise Rep. 53*, 129 pp., Natl. Oceanogr. Cent. Southampton, Southampton, U. K.

Barrier, N., J. Deshayes, A.-M. Treguier, and C. Cassou (2015), Heat budget in the North Atlantic subpolar gyre: Impacts of atmospheric weather regimes on the 1995 warming event, *Prog. Oceanogr.*, *130*, 75–90.

Bauch, D., M. R. van der Loeff, N. Andersen, S. Torres-Valdes, K. Bakker, and E. P. Abrahamsen (2011), Origin of freshwater and polynya water in the Arctic Ocean halocline in summer 2007, *Prog. Oceanogr.*, *91*(4), 482–495, doi:10.1016/j.pocean.2011.07.017.

Belkin, I. M., S. Levitus, J. Antonov, and S.-A. Malmberg (1998), Great salinity anomalies in the North Atlantic, *Prog. Oceanogr.*, *41*(1), 1–68.

Benetti, M., G. Reverdin, C. Pierre, S. Khatiwala, B. Tournadre, S. Olafsdottir, and A. Naamar (2016), Variability of sea ice melt and meteoric water input in the surface Labrador Current off Newfoundland, *J. Geophys. Res. Oceans*, *121*, 2841–2855, doi:10.1002/2015JC011302.

Brodeau, L., B. Barnier, A.-M. Treguier, T. Penduff, and S. Gulev (2010), An ERA40-based atmospheric forcing for global ocean circulation models, *Ocean Modell.*, *31*(3), 88–104.

Cooper, L. W., T. E. Whitledge, J. M. Grebmeier, and T. Weingartner (1997), The nutrient, salinity, and stable oxygen isotope composition of Bering and Chukchi Seas waters in and near the Bering Strait, *J. Geophys. Res.*, *102*(C6), 12,563–12,573.

Cooper, L. W., L. A. Codispoti, V. Kelly, G. G. Sheffield, and J. M. Grebmeier (2006), The potential for using Little Diomede Island as a platform for observing environmental conditions in Bering Strait, *Arctic*, *59*, 129–141.

Cooper, L. W., J. W. McClelland, R. M. Holmes, P. A. Raymond, J. J. Gibson, C. K. Guay, and B. J. Peterson (2008), Flow-weighted values of runoff tracers (δ^{18}O, DOC, Ba, alkalinity) from the six largest Arctic rivers, *Geophys. Res. Lett.*, *35*, L18606, doi:10.1029/2008GL035007.

Cox, K. A., J. D. Stanford, A. J. McVicar, E. J. Rohling, K. J. Heywood, S. Bacon, M. Bolshaw, P. A. Dodd, S. De la Rosa, and D. Wilkinson (2010), Interannual variability of Arctic sea ice export into the East Greenland Current, *J. Geophys. Res.*, *115*, C12063, doi:10.1029/2010JC006227.

Curry, B., C. M. Lee, B. Petrie, R. E. Moritz, and R. Kwok (2014), Multiyear volume, liquid freshwater, and sea ice transports through Davis Strait, 2004–10, *J. Phys. Oceanogr.*, *44*(4), 1244–1266.

Dansgaard, W. (1964), Stable isotopes in precipitation, *Tellus*, *16*(4), 436–468.

Dickson, R. R., J. Meincke, S.-A. Malmberg, and A. J. Lee (1988), The "great salinity anomaly" in the northern North Atlantic 1968–1982, *Prog. Oceanogr.*, *20*(2), 103–151.

Dodd, P. A., B. Rabe, E. Hansen, E. Falck, A. Mackensen, E. Rohling, C. Stedmon, and S. Kristiansen (2012), The freshwater composition of the Fram Strait outflow derived from a decade of tracer measurements, *J. Geophys. Res.*, *117*, C11005, doi:10.1029/2012JC008011.

Falkowski, P. G., and C. S. Davis (2004), Natural proportions, *Nature*, *431*(7005), 131–131.

Fratantoni, P. S., and M. S. McCartney (2010), Freshwater export from the Labrador Current to the North Atlantic Current at the Tail of the Grand Banks of Newfoundland, *Deep Sea Res., Part I*, *57*(2), 258–283.

Grégorio, S., T. Penduff, G. Sérazin, J.-M. Molines, B. Barnier, and J. Hirschi (2015), Intrinsic variability of the Atlantic meridional overturning circulation at interannual-to-multidecadal time scales, *J. Phys. Oceanogr.*, *45*(7), 1929–1946, doi:10.1175/JPO-D-14-0163.1.

Jones, E. P., L. G. Anderson, and J. H. Swift (1998), Distribution of Atlantic and Pacific waters in the upper Arctic Ocean: Implications for circulation, *Geophys. Res. Lett.*, *25*(6), 765–768.

Jones, E. P., L. G. Anderson, S. Jutterström, L. Mintrop, and J. H. Swift (2008), Pacific freshwater, river water and sea ice meltwater across Arctic Ocean basins: Results from the 2005 Beringia Expedition, *J. Geophys. Res.*, *113*, C08012, doi:10.1029/2007JC004124.

Kieke, D., and I. Yashayaev (2015), Studies of Labrador Sea Water formation and variability in the subpolar North Atlantic in the light of international partnership and collaboration, *Prog. Oceanogr.*, *132*, 220–232.

King, B. A., et al. (2015), RRS James Clark Ross Cruise 302, 06 Jun–21 Jul 2014, *The 2015 RAGNARRoC, OSNAP and Extended Ellett Line Cruise Rep. 35*, 76 pp., Natl. Oceanogr. Cent., Southampton, U. K.

Khatiwala, S. P., R. G. Fairbanks, and R. W. Houghton (1999), Freshwater sources to the coastal ocean off northeastern North America: Evidence from H2 18O/H2 16O, *J. Geophys. Res.*, *104*(C8), 18,241–18,255.

Kwok, R., and D. A. Rothrock (1999), Variability of Fram Strait ice flux and North Atlantic Oscillation, *J. Geophys. Res.*, *104*(C3), 5177–5189.

Kwok, R., and D. A. Rothrock (2009), Decline in Arctic sea ice thickness from submarine and ICESat records: 1958–2008, *Geophys. Res. Lett.*, *36*, L15501, doi:10.1029/2009GL039035.

Lazier, J., R. Hendry, A. Clarke, I. Yashayaev, and P. Rhines (2002), Convection and restratification in the Labrador Sea, 1990–2000, *Deep Sea Res. Part I*, *49*(10), 1819–1835.

Lazier, J. R. N. (1973), The renewal of Labrador Sea water, *Deep Sea Res. Oceanogr. Abstr.*, *20*, 341–353.

Lécuyer, C., V. Gardien, T. Rigaudier, F. Fourel, F. Martineau, and A. Cros (2009), Oxygen isotope fractionation and equilibration kinetics between CO_2 and H_2O as a function of salinity of aqueous solutions, *Chem. Geol.*, *264*(1), 122–126.

Lilly, J. M., P. B. Rhines, M. Visbeck, R. Davis, J. R. Lazier, F. Schott, and D. Farmer (1999), Observing deep convection in the Labrador Sea during winter 1994/95, *J. Phys. Oceanogr.*, *29*(8), 2065–2098.

Lique, C., and M. Steele (2013), Seasonal to decadal variability of Arctic Ocean heat content: A model-based analysis and implications for autonomous observing systems, *J. Geophys. Res. Oceans*, *118*, 1673–1695, doi:10.1002/jgrc.20127.

Lique, C., A.-M. Tréguier, M. Scheiner, and T. Penduff (2009), A model-based study of ice and freshwater transport variability along both sides of Greenland, *Clim. Dyn.*, *33*, 685–705, doi:10.1007/s00382-008-0510-7.

Lique, C., A.-M. Treguier, B. Blanke, and N. Grima (2010), On the origins of water masses exported along both sides of Greenland: A Lagrangian model analysis, *J. Geophys. Res.*, *115*, C05019, doi:10.1029/2009JC005316.

McGeehan, T., and W. Maslowski (2011), Impact of shelf-basin freshwater transport on deep convection in the western Labrador Sea, *J. Phys. Oceanogr.*, *41*(11), 2187–2210.

Melling, H., and R. M. Moore (1995), Modification of halocline source waters during freezing on the Beaufort Sea shelf: Evidence from oxygen isotopes and dissolved nutrients, *Cont. Shelf Res.*, *15*(1), 89–113.

Mertz, G., S. Narayanan, and J. Helbig (1993), The freshwater transport of the Labrador Current, *Atmos. Ocean*, *31*(2), 281–295.

Michel, C., J. Hamilton, E. Hansen, D. Barber, M. Reigstad, J. Iacozza, L. Seuthe, and A. Niemi (2015), Arctic Ocean outflow shelves in the changing Arctic: A review and perspectives, *Prog. Oceanogr.*, *139*, 66–88.

Münchow, A. (2016), Volume and freshwater flux observations from Nares Strait to the west of Greenland at daily time scales from 2003 to 2009, *J. Phys. Oceanogr.*, *46*(1), 141–157.

Myers, R. A., S. A. Akenhead, and K. Drinkwater (1990), The influence of Hudson Bay runoff and ice-melt on the salinity of the inner Newfoundland Shelf, *Atmos. Ocean*, *28*(2), 241–256.

Östlund, H. G., and G. Hut (1984), Arctic Ocean water mass balance from isotope data, *J. Geophys. Res.*, *89*(C4), 6373–6381.

Petrie, B., S. A. Akenhead, S. A. Lazier, and J. Loder (1988), The cold intermediate layer on the Labrador and Northeast Newfoundland Shelves, 1978–86, *NAFO Sci. Counc. Stud.*, *12*, 57–69.

Rabe, B., P. A. Dodd, E. Hansen, E. Falck, U. Schauer, A. Mackensen, A. Beszczynska-Möller, G. Kattner, E. J. Rohling, and K. Cox (2013), Liquid export of Arctic freshwater components through the Fram Strait 1998–2011, *Ocean Sci.*, *9*(1), 91–109.

Rahmstorf, S., G. Feulner, M. E. Mann, A. Robinson, S. Rutherford, and E. J. Schaffernicht (2015), Exceptional twentieth-century slowdown in Atlantic Ocean overturning circulation, *Nat. Clim. Change*, *5*, 475–480.

Redfield, A. C. (1958), The biological control of chemical factors in the environment, *Am. Sci.*, *46*(3), 230A–221.

Redfield, A. C. (1963), The influence of organisms on the composition of sea-water, in *The Sea*, vol. II, edited by M. N. Hill, pp. 26–77, John Wiley, New York.

Reverdin, G. (2003), North Atlantic Ocean surface currents, *J. Geophys. Res.*, *108*(C1), 3002, doi:10.1029/2001JC001020.

Schmidt, G. A., G. R. Bigg, and E. J. Rohling (1999), Global Seawater Oxygen-18 Database-v1.21. [Available at http://data.giss.nasa.gov/o18data/, NASA.]

Shepherd, A., et al. (2012), A reconciled estimate of ice-sheet mass balance, *Science*, *338*(6111), 1183–1189.

Skrzypek, G., and D. Ford (2014), Stable isotope analysis of saline water samples on a cavity ring-down spectroscopy instrument, *Environ. Sci. Technol.*, *48*(5), 2827–2834.

Steur, L., R. S. Pickart, D. J. Torres, and H. Valdimarsson (2015), Recent changes in the freshwater composition east of Greenland, *Geophys. Res. Lett.*, *42*, 2326–2332, doi:10.1002/2014GL062759.

Straneo, F. (2006), Heat and freshwater transport through the Central Labrador Sea, *J. Phys. Oceanogr.*, *36*(4), 606–628.

Straneo, F., and F. Saucier (2008), The outflow from Hudson Strait and its contribution to the Labrador Current, *Deep Sea Res., Part I*, *55*(8), 926–946.

Sutherland, D. A., R. S. Pickart, E. Peter Jones, K. Azetsu-Scott, A. Jane Eert, and J. Ólafsson (2009), Freshwater composition of the waters off southeast Greenland and their link to the Arctic Ocean, *J. Geophys. Res.*, *114*, C05020, doi:10.1029/2008JC004808.

Taylor, J. R., Falkner, K. K., U. Schauer, and M. Meredith (2003), Quantitative considerations of dissolved barium as a tracer in the Arctic Ocean, *J. Geophys. Res.*, *108*(C12), 3374, doi:10.1029/2002JC001635.

Tremblay, J.-É., L. G. Anderson, P. Matrai, P. Coupel, S. Bélanger, C. Michel, and M. Reigstad (2015), Global and regional drivers of nutrient supply, primary production and CO 2 drawdown in the changing Arctic Ocean, *Prog. Oceanogr.*, *139*, 171–196.

Våge, K., R. S. Pickart, A. Sarafanov, Ø. Knutsen, H. Mercier, P. Lherminier, H. M. van Aken, J. Meincke, D. Quadfasel, and S. Bacon (2011), The Irminger Gyre: Circulation, convection, and interannual variability, *Deep Sea Res., Part I*, *58*(5), 590–614.

van der Broeke, M., E. Enderli, I. Howat, P. K. Munneke, B. Noël, W. van de Berg, E. van Meijgaard, and B. Wouters (2016), On the recent contributions of the Greenland ice sheet to sea level change, *Cryosphere*, *10*, 1933–1946, doi:10.5194/tc-2016-123.

Woodgate, R. A., and K. Aagaard (2005), Revising the Bering Strait freshwater flux into the Arctic Ocean, *Geophys. Res. Lett.*, *32*, L02602, doi: 10.1029/2004GL021747.

Woodgate, R. A., T. J. Weingartner, and R. Lindsay (2012), Observed increases in Bering Strait oceanic fluxes from the Pacific to the Arctic from 2001 to 2011 and their impacts on the Arctic Ocean water column, *Geophys. Res. Lett.*, *39*, L24603, doi:10.1029/2012GL054092.

Wu, Y., C. Tang, and C. Hannah (2012), The circulation of eastern Canadian seas, *Prog. Oceanogr.*, *106*, 28–48.

Yamamoto-Kawai, M., F. A. McLaughlin, E. C. Carmack, S. Nishino, and K. Shimada (2008), Freshwater budget of the Canada Basin, Arctic Ocean, from salinity, δ^{18}O, and nutrients, *J. Geophys. Res.*, *113*, C01007, doi:10.1029/2006JC003858.

Yashayaev, I. (2007), Hydrographic changes in the Labrador Sea, 1960–2005, *Prog. Oceanogr.*, *73*(3), 242–276.

Yashayaev, I., and J. W. Loder (2009), Enhanced production of Labrador Sea water in 2008, *Geophys. Res. Lett.*, *36*, L01606, doi:10.1029/2008GL036162.

Yashayaev, I., H. M. van Aken, N. P. Holliday, and M. Bersch (2007), Transformation of the Labrador sea water in the subpolar North Atlantic, *Geophys. Res. Lett.*, *34*, L22605, doi:10.1029/2007GL031812.

Yashayaev, I., D. Seidov, and E. Demirov (2015), A new collective view of oceanography of the Arctic and North Atlantic basins, *Prog. Oceanogr.*, *21*, 1–21, doi:10.1016/j.pocean.2014.12.012.